Ecography

ECOG-03655
Barton, M. G., Clusella-Trullas, S. and Terblanche, J. S. 2018. Spatial scale, topography and thermoregulatory behaviour interact when modelling species' thermal niches. – Ecography doi: 10.1111/ecog.03655

Supplementary material

Appendix 1

Detailed description of the biophysical model.

Climate data preparation

To simulate diurnal temperature fluctuations and attain measures of ambient temperature on hourly time steps throughout the year, we splined average monthly minimum and maximum temperature datasets into 365 days. These daily temperature measures were subsequently interpolated with a sinusoidal wave to generate hourly temperature profiles, according to the equation in Campbell and Norman (1998).

First, the dimensionless diurnal temperature function (Γ) was calculated:

$$\Gamma(t) = 0.44 - 0.46\sin(\omega t + 0.9) + 0.11\sin(2\omega t + 0.9)$$

where ω is $\pi/12$, t is the time of day in hours. The ambient temperature at hourly time steps was then determined by

$$\mathrm{Ta(hour)} \begin{cases} T_{x,i-1}\Gamma(t) + T_{n,i}[1 - \Gamma(t)] & 0 < t \leq 5 \\ T_{x,i}\Gamma(t) + T_{n,i}[1 - \Gamma(t)] & 5 > t \leq 14 \\ T_{n,i}\Gamma(t) + T_{n,i+1}[1 - \Gamma(t)] & 14 < t < 24 \end{cases}$$

where T_x is the daily maximum temperature, T_n the daily minimum temperature, both of which were sourced from the *Worldclim* database, Version 1.4 (Hijmans et al., 2005); http://www.worldclim.org/current.htm), and i represents the day of the year (such that $(i - 1)$ is the previous day and $(i + 1)$ the following day).

Measurements of average monthly relative humidity, sourced from Schulze (1997), were also splined across 365 days to attain average daily measures, which were assumed to remain constant throughout the day.

Topographical effects on microclimates

Topographical features can have substantial impacts on exposure to solar radiation, and consequently the body temperature of the animal. For each day, and at each location across our modelling extent, we calculated the position of the sun in the sky at hourly intervals, again, based on calculations described in Campbell and Norman (1998).

Briefly, the sun's location in the sky depends on the hour of the day, the day of the year ("Julian day" hereafter), and the latitude and longitude of the site.

The sun's declination angle (Φ) for any given day of the year (d) is first calculated by:

$$\Phi = -0.39785 \times \sin(278.97 + (0.9856d)) + 1.9165 \times \sin(356.6 + 0.9856d)$$

The solar zenith (z) at each hour of the day (h) at any given latitude (δ) is then determined by:

$$\cos z = \sin\delta \sin\Phi + \cos\delta \cos\Phi \cos h$$

Drawing on these zenith and declination values, as well as latitude, the sun's azimuth (α), the angle of direct solar radiation around true north, can then be calculated with (where zenith, declination and latitude are in radians):

$$\cos\alpha = \frac{\cos z \sin\delta - \sin\Phi}{\sin z \cos\delta}$$

For the southern hemisphere latitude is defined with negative values, such that the azimuth and zenith at true solar noon are both zero.

Once the sun's location is known, direct solar radiation (S_{dir}) is calculated when the sun is above the horizon (z <90), while accounting for atmospheric transmittance (see Campbell and Norman, 2008). Direct solar radiation is thus calculated according to:

$$S_{dir} = S_0 \times \tau^m$$

Where S_0 is the extra-terrestrial flux density (1360Wm^{-2}), τ is the atmospheric transmittance (here assumed to be 0.6, reflecting clear skies), and m is the optimal mass number for the given location. This latter term depends on the atmospheric pressure of the location (p_a) determined from relative humidity.

$$m = \frac{p_a}{101.3 \times \cos(z)}$$

Optimal mass varies with elevation, but only for locations in excess of 6000 m.a.s.l, beyond the scope of our modelling extent.

Diffuse radiation loads were also calculated according to:

$$S_{diff} = 0.3 * S_0 * \cos(z) * (1 - \tau^m)$$

And reflected solar radiation, assuming a surface albedo of 0.1, determined by:

$$S_{ref} = (S_{dir} + S_{diff}) * \text{albedo}$$

At this stage, topographical features of the landscape can be incorporated into the model to account for their effect on solar radiation loads. Specifically, slope and aspect alter the view factors for direct, diffuse and reflected solar radiation (F_I , F_D and F_R respectively). These view factors were calculated according to each location's (grid cell's) slope and aspect according to:

$$F_I = \cos(\text{slope}) * \cos(z) + \sin(\text{slope}) * \sin(z) * \cos(\alpha - \text{aspect})$$

$$F_R, F_D = 1 + \frac{\cos(\text{slope})}{2}$$

And calculated levels of solar radiation were adjusted accordingly:

$$S_{dir} = S_{dir} \times F_I$$

$$S_{diff} = S_{diff} \times F_D$$

$$S_{ref} = S_{ref} \times F_R$$

Finally, shading at each location from adjacent topographical features needed to be accounted for, by if the sun was above, or below the horizon at each location. For each hour of the day, the local horizon angle in the direction of the sun's azimuth angle was first determined. If this horizon angle was higher than the sun's elevation $(90 - z)$ at that particular hour, the sun was deemed to be below the horizon, and as a consequence, $S_{dir} = 0$ (the site was shaded from direct solar radiation).

Modelling microclimates

Each life-history stage was assumed to be in one of three microclimates: on the surface of a leaf within the canopy (eggs and larvae), buried 5cm under the substrate (pupae) or perched at half a metre high on the trunk of a tree (adults).

In all microclimates, we assumed that the effects of heat exchange between *H. armigera* and its environment through evaporation, and any heat generated in the animal through metabolism, were negligible (Watt, 1968; Rawlins, 1980; Kingsolver & Moffat, 1982).

Therefore, operative body temperature (Te) was calculated within each microclimate according to:

$$Te = Ta + \frac{R_n - \sigma\varepsilon(Ta + 273.15)^4}{c_p(g_r + g_{Ha})}$$

where Ta is the ambient temperature at the height of the animal; R_n is net radiation heat flux; σ is the Stefan-Boltzman constant (5.67×10^{-8} $Wm^{-2}K^{-4}$); ε is the emissivity of the *H. armigera* (0.97); c_p is the specific heat content of the air (29.3 Jkg^{-1} K^{-1}); g_r is radiative conductance of *H. armigera*; and finally, g_{Ha} is the boundary layer conductance of heat (Wm^{-1} K^{-1}), both of which depend on the ambient temperature of the Bollworm.

For terrestrial microclimates (of the eggs, larvae and adults), ambient temperature varies with height above the substrate, and so Ta was adjusted for the height of the animal according to a well-established temperature profile equation (Campbell & Norman, 1998):

$$T(h) = T_0 - \frac{H}{0.4\hat{\rho}c_p u^*} \ln\frac{z - d}{z_H}$$

Where T_0 is the apparent aerodynamic surface temperature, H is the sensible heat flux, $\hat{\rho}c_p$ is the volumetric specific heat content of air ($1200Jm^{-3}°C^{-1}$ at 20°C and at sea level), u^* is the friction velocity at the reference height and finally, z_H is the roughness parameter of the substrate (here assumed to be 5cm high).

Once the ambient temperature at the height of the eggs, larvae and pupae was determined, additional heat gain through radiation and conduction, and heat lost through convection were considered for each location.

An Apple-Tree Trunk

Adults perched at a height of 0.5 m on the trunk of the tree were assumed to be perpendicular to direct solar beam at all times

Diffuse (S_{diff}) and reflected (S_{ref}) solar radiation loads were calculated according to the view factor of each site, and assuming an albedo for bare soil of 0.1 (see above). Short wave radiation loads (SR_{abs}) absorbed by the adult moth on the trunk were then calculated by:

$$SR_{abs} = 0.5A * \alpha_s S_{dir} + \alpha_s S_{diff} + \alpha_s S_{ref}$$

where α_s is the absorptivity of short-wave radiation of the thorax (0.95) and A is the total surface area of the bollworm (we assumed that half of the animal's surface area was exposed to the direct solar beam).

To calculate infrared radiation emitted from the trunk (IR_{trunk}) its surface temperature was required. We calculated tree-trunk surface temperature (T_{trunk}) assuming that the centre of the trunk was the same temperature as 2m below the soil (see equation below), and heat was conducted between the trunk centre and its surface according to equations defined in Derby and Gates (1966) and Potter and Andresen (2002). With this prediction of T_{trunk}, emitted long-wave radiation was determined:

$$IR_{trunk} = \sigma(T_{trunk} + 273)^4$$

This value was combined with values of long-wave radiation emitted from the ground and (a cloudless) sky (Campbell and Norman, 1998), and assuming that half of *H. armigera*'s thorax is exposed to each:

$$IR_{abs} = 0.5\alpha_l(IR_{trunk} + IR_{sky} + IR_{ground})$$

where α_l is the absorptivity of the thorax of long-wave radiation. Net radiation heat flux was thus:

$$R_n = SR_{abs} + IR_{abs}$$

Wind speed (u) on the trunk was assumed to be 0.5ms^{-1} at all times, and so the boundary layer conductance of heat was calculated from:

$$g_{Ha} = 1.4 \cdot 0.135 \cdot \sqrt{\frac{u}{L_D}}$$

where L_D is the characteristic dimension of the (cylindrical) adult, determined by

$$L_D = Volume^{1/3}$$

Finally, radiative conductance of the bollworm was calculated by:

$$g_r = \frac{4\sigma\,(Ta + 273.15)^3}{c_p}$$

and Te was calculated using the energy balance equation described above.

A leaf in the canopy

Eggs and larvae on a leaf surface within the canopy (2m above the substrate) were assumed to be at the temperature of the leaf tissue. To calculate leaf surface temperatures we determined the latent heat flux, sensible heat flux and net radiation according to Pincebourde and Casas (2006). Net radiation absorbed by a leaf depends largely on the nature of the surrounding canopy, particularly with respect to radiation loads (Pincebourde et al., 2007). We assumed the apple canopy best approximates a sphere (Green & McNaughton, 1997), and so the amount of solar radiation that penetrates through the canopy was determined by:

$$S_{dir.canopy} = S_{dir} * \theta_b$$

where θ_b, defines the fraction of a direct solar radiation beam that penetrates through the canopy, was calculated from:

$$\theta_b = e^{-K_b \cdot LAI}$$

Where the leaf area index (LAI) was assumed to be 2.0 (Palmer et al., 1992), the extinction factor K_b calculated by:

$$K_b = \frac{1}{2 * \cos(z)}$$

Once this was determined, we could calculate the diffuse radiation scattered from the surrounding leaves within the canopy,

$$S_{diff.canopy} = S_{diff} * \ (1 - e^{(-1\sqrt{\alpha_L} * K_b * height)})$$

in which α_L is the absorptivity of the leaf (0.84), and $height$ represents the depth of the leaf within the canopy. Finally, the reflected radiation absorbed by the leaf at a specified height within the canopy was determined from the equation above, but K_b was replaced with K_d, the extinction factor for diffuse radiation. See Campbell and Gates (1998, page 254) for further information.

Heat gained and lost at the surface of the leaf through processes of conduction and convection were determined according to calculations in Pincebourde and Casas (2006), along with standard parameters for a leaf defined in Campbell and Gates (1998, Chapter 14).

Below the substrate

We assumed that pupae were buried 5cm below the substrate and that (Te) was at equilibrium with soil temperature (Campbell and Norman 1998, Fig. 1b, also Chapter 8). The temperature of the soil (assumed to be of organic composition), at this depth (z) was calculated from:

$$T_e = T_{soil} + Amp * e^{-z/D} * \sin[\omega(hour - 8) - z/D]$$

where T_{soil} is the mean substrate temperature throughout the day, and Amp is the amplitude of diurnal substrate temperature fluctuations around this mean. Here, daily substrate maximum and minimum temperatures were assumed to be half a degree lower and higher than daily maximum and minimum air temperatures respectively (Wu & Nofziger, 1999). The damping depth D was calculated according to:

$$D = \sqrt{\frac{2\kappa}{\omega}}$$

where κ is the soil diffusivity m^2s^{-1}, and $\omega = 7.3 \times 10^{-5}s^{-1}$.

Bollworm fitness and survival

Data on the number of degree-days required to complete development for each of the life-history stages of *H. armigera* were sourced from previous studies (Mironidis & Savopoulou-Soultani, 2008; Mironidis, 2014) and adjusted to account for the hourly (rather than daily) time steps. The minimum (T_{min}) and maximum (T_{max}) developmental thresholds were also obtained from previous work on this species studies (Mironidis & Savopoulou-Soultani, 2008; Mironidis, 2014). For each hour of the simulations, if predicted T_e was between the T_{min} and CT_{max}, the number of degree-day units accumulated on that time-step were calculated from:

$$\text{Degree. Days} = T_e - T_{min}$$

All scripts were written, and model simulations run, in R (Version 3.1.2.) and are available from the authors upon request.

References

Campbell, G.S. & Norman, J.M. (1998) An Introduction of Evnironmental Biophysics; Second Edition. Springer Science, New York, USA.

Derby, R.W. & Gates, D.M. (1966) The temperature of tree trunks-calculated and observed. American Journal of Botany, **53**, 580-587.

Green , S.R. & McNaughton, K.G. (1997) Modelling effective stomata1 resistance for calculating transpiration from an apple tree. Agricultural and Forest Meteorology, **83**, 1-26.

Hijmans, R.J., Cameron, S.E., Parra, J.L., Jones, P.G. & Jarvis, A. (2005) Very high resolution interpolated climate surfaces for global land areas. International Journal of Climatology, **25**, 1965-1978.

Kingsolver, J.G. & Moffat, R.J. (1982) Thermoregulation and the determinants of heat transfer in Colias butterflies. Oecologia, **53**, 27-33.

Mironidis, G.K. (2014) Development, survivorship and reproduction of Helicoverpa armigera (Lepidoptera: Noctuidae) under fluctuating temperatures. Bulletin of Entomological Research, **104**, 751–764.

Mironidis, G.K. & Savopoulou-Soultani, M. (2008) Development, survivorship, and reproduction of Helicoverpa armigera (Lepidoptera: Noctuidae) under constant and alternating temperatures. Environmental Entomology of America, **37**, 16-28.

Palmer, J.W., Avery, D.J. & Wertheim, S.J. (1992) Effect of apple tree spacing and summer pruning on leaf area distribution and light interception. Scientia Horticulturae, **52**, 303-312.

Pincebourde, S. & Casas, J. (2006) Multitrophic biphysical budgets: thermal ecology of an intimate herbivore insect-plant interaction. Ecological Monographs, **76**, 175–194.

Pincebourde, S., Sinoquet, H., Combes, D. & Casas, J. (2007) Regional climate modulates the canopy mosaic of favourable and risky microclimates for insects. Journal of Animal Ecology, **76**, 424–438.

Potter, B.E. & Andresen, J.A. (2002) A finite-difference model of temperatures and heat flow within a tree stem. Can. J. For. Res., **32**, 548–555.

Rawlins, J.E. (1980) Thermoregulation by the Black Swallowtail butterfly, Papilio polyxenes (Lepidoptera: Pappilionidae). Ecology, **6**, 345-357.

Schulze, R.E. (1997) South African atlas of agrohydrology and climatology. In: Report TT 82/96. Water Research Commission, Pretoria.

Watt, W.B. (1968) Adaptive significance of pigment polymorphisms in Colias Butterflies. I. Variation of melanin pigment in relation to thermoregulation. Evolution **22**, 437 - 458.

Wu, J. & Nofziger, D.L. (1999) Incorporating temperature effects on pesticide degradation into a management model. Journal of Environmental Quality, **28**, 92-100.

Appendix 2

Additional Figures and Tables

Figure A1 Schematic showing how the cells were aggregated from (a) fine, into (b) medium and (c) coarse resolutions. The aggregate function in the Raster package for R calculates the mean values for elevation and each climatic variable across 4 and 9 adjacent fine-grid cells for the medium and coarse resolutions respectively, where the top-left hand cell remains aligned in all resolutions.

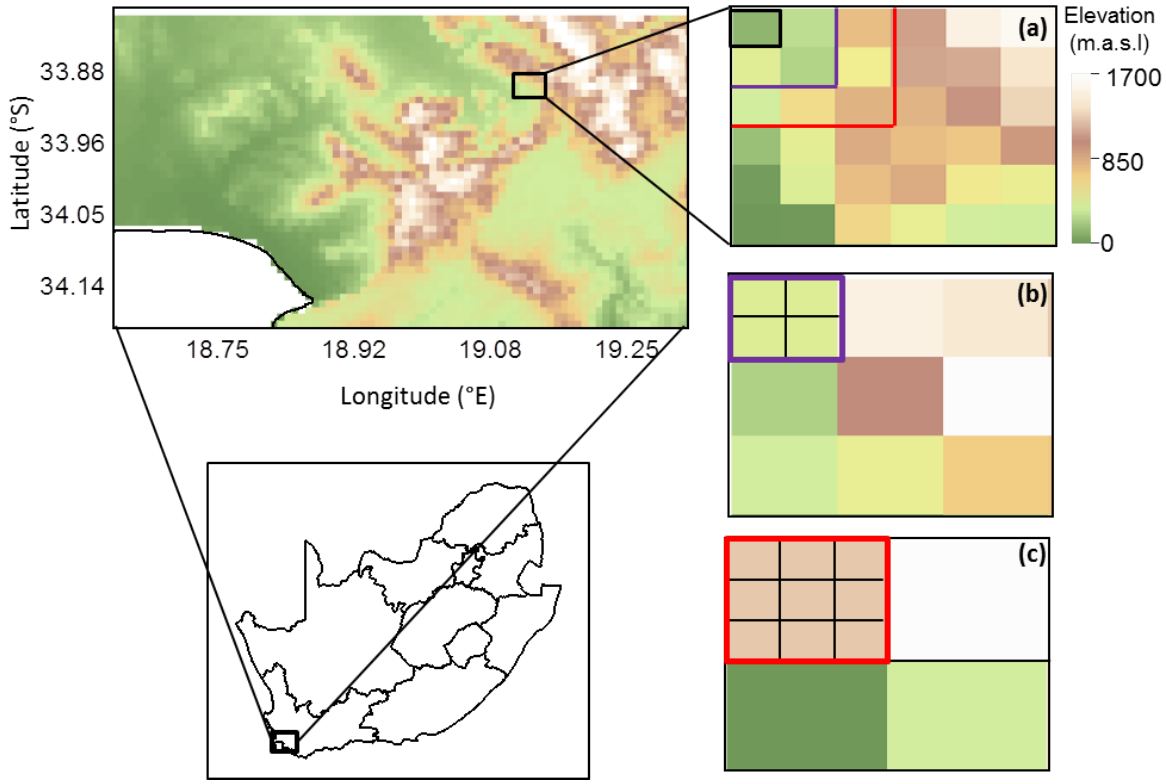

Figure A2. Variation in slope (a), and corresponding average (b) direct and (c) diffuse solar radiation loads with increasing elevation. Predictions for coarse (black, solid) and fine (grey, stipled) scale simulations are shown. At high elevations, the coarse resolution had relatively steeper slopes and received higher levels of direct radiation than the same locations modelled at a fine resolution. This process is likely to have led to variation in predicted operative temperatures and predicted thermal niches of the species.

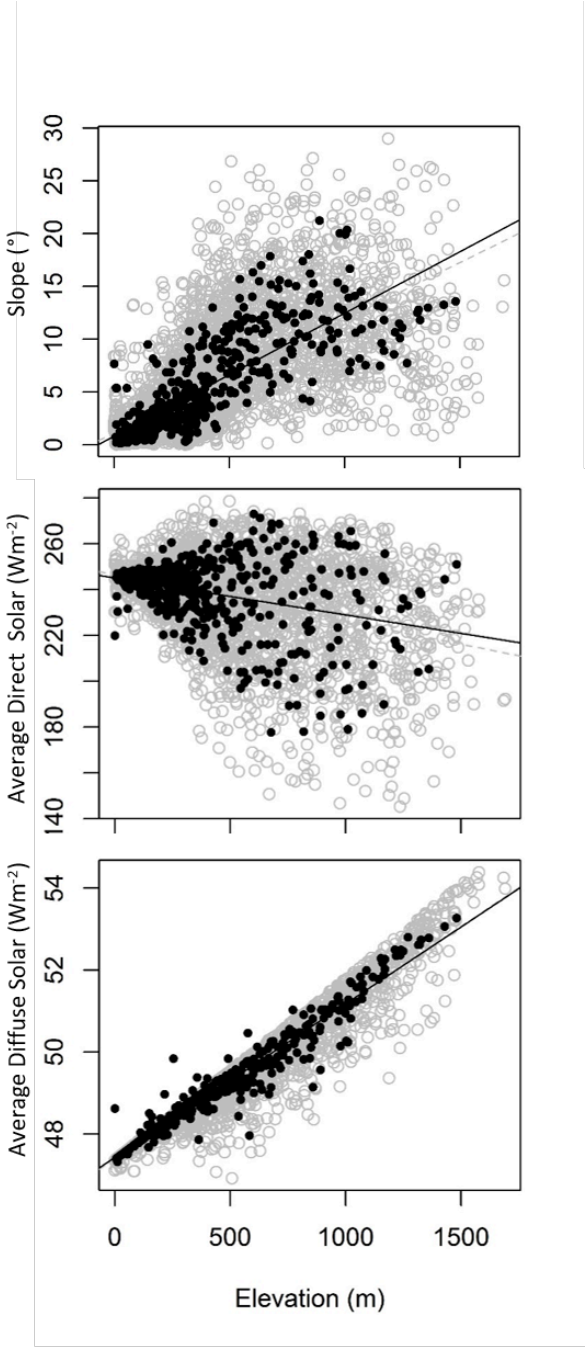

Table A1. Stage-specific physiological rates and thresholds for *Helicoverpa armigera*, used by the model to represent a cosmopolitan holometabolous insect. The total number of degree-day units required to complete each stage (K), the thermal thresholds for development (T_{min} and T_{max}, °C), as well as the microclimate of each stage are listed.

Stage	K	T_{min}	T_{max}	Microclimate
Egg	1090	10.8	40	Leaf
Larva	4800	13.6	40	Leaf
Pupa	3428	14.6	40	Underground
Adult	100	12	40	Tree Trunk

Appendix 3

Additional simulations across agricultural regions

Methods

To confirm that the discrepancies in predicted T_e (and associated traits) detected at different spatial scales in the Western Cape of South Africa were not specific to that particular region, we ran some additional model simulations. Four additional regions were chosen across the globe were chosen. *Helicoverpa armigera* is a pest in apple orchards in the Western Cape, and so apple growing regions were chosen. We considered Mediterranean Europe; Tasmania, Australia; Shandon, China and California, USA. Each region covered a gradient in elevation (see Fig. 5a,c,e,g. in manuscript).

Two sets of simulations were run as described in the body of the manuscript, however *Worldclim* data at a 10 arc-minute resolution (coarse scale) and 5 arc-minute resolution (fine scale) were included as input climate data. Due to time limitations, simulations were run for 24 hours only, using climate data for the 1st July, capturing mid-summer and mid-winter in the northern, and winter in the southern hemisphere.

We built generalized linear mixed effects models (GLMMs) to test the impacts of topography and spatial-scale on the model's prediction of T_e across each region. As described in the manuscript, we first built full models with interactions between scale, elevation, aspect and slope, and then sequentially removed non-significant parameters until the model of best fit was achieved, according to the lowest BIC value. For all models, site (or grid cell) was included as a random factor to account for pseudo-replication among the fine and coarse data. To remove confounding effects of spatial correlation among sites within each region, an auto-covariate term was included in the model (see paper for further details). Multi-collinearity

and spatial autocorrelation of the final model of best fit were again checked, according to methods described in the manuscript.

Results

Discrepancies in T_e predictions between the coarse and fine-scale simulations across the four regions depended on slope and elevation of each grid cell. As was observed for the Western Cape Province in South Africa, at low elevations, the coarse resolution under-predicted T_e, but over-predicted T_e at higher elevations, in comparison to the fine-scale resolution (Table1; Fig. 5 b, d, f, h of manuscript). For all regions, these discrepancies were greatest on steep, as opposed to shallow slopes. While the extent of these discrepancies varied to some degree among regions (note the different scale on the y-axis in Figure 5,b, d, f, h of manuscript) the overall, consistent among different regions, confirms that the model predictions hold across multiple regions, spatial, and temporal scales.

Table A1. Results of generalized linear mixed effects models for the differences between coarse and fine-scale resolution predictions of average T_e. Estimates are shown for each parameter and significance represented with ***($p<0.001$); **($p<0.01$; *($p<0.05$)

	Tasmania, Australia	*Mediterranean Europe*	*California, USA*	*Shandon, China*
Intercept	$2.987(\pm7.446\times10^{-3})$***	$3.16(\pm6.561\times10^{-3})$***	$2.818(\pm0.012)$***	$3.266(\pm3.471\times10^{-3})$***
Elevation	$-2.266\times10^{-3}(\pm9.33\times10^{-5})$***	$-1.209\times10^{-3}(\pm3.681\times10^{-5})$***	$5.707\times10^{-4}(\pm5.266\times10^{-5})$***	-1.484×10^{-3} $(\pm3.637\times10^{-3})$***
Slope	$-7.587\times10^{-3}(\pm3.997\times10^{-3})$	$0.053(\pm1.529\times10^{-3})$***	$1.903\times10^{-3}(\pm2.997\times10^{-3})$	$-0.02445\times10^{-3}(1.615\times10^{-3})$***
Aspect	$1.168\times10^{-3}(\pm3.136\times10^{-3})$	$0.016(\pm1.913\times10^{-3})$***	$0.01271(\pm5.79\times10^{-3})$*	$-4.151\times10^{-3}(\pm1.217\times10^{-3})$***
Scale	$-2.193\times10^{-3}(\pm1.971\times10^{-3})$	$-3.962\times10^{-4}(\pm2.545\times10^{-4})$	$2.033\times10^{-3}(\pm0.0005727\times10^{-3})$***	$9.638\times10^{-5}(\pm1.191\times10^{-6})$
Auto-covariate	$-2.758\times10^{3}(\pm5621)$***	$6.942\times10^{-3}(\pm4.617\times10^{-3})$	$0.066(\pm1.354\times10^{-3})$***	$0.014(\pm3.119\times10^{-4})$***
Elevation^2	-1.289×10^{-5} $(\pm1.067\times10^{-6})$***	$-2.666\times10^{-6}(\pm2.361\times10^{-7})$***	$-7.416\times10^{-6}(\pm3.342\times10^{-7})$***	$-4.01\times10^{-6}(\pm3.025\times10^{-7})$
Elevation × Slope	-1.101×10^{-4} $(\pm7.896\times10^{-5})$	$-3.642\times10^{-4}(\pm1.656\times10^{-5})$***	$-2.918\times10^{-5}(\pm2.248\times10^{-6})$	$8.242\times10^{-5}(\pm3.022\times10^{-6})$**
Elevation × Aspect	$-3.784\times10^{-4}(\pm8.122\times10^{-5})$***	$2.24\times10^{-4}(\pm3.512\times10^{-5})$	$-5.586\times10^{-4}(\pm5.063\times10^{-5})$	$-5.574\times10^{-4}(\pm3.404\times10^{-5})$
Scale × Elevation	$2.512\times10^{-4}(\pm4.335\times10^{-5})$***	$1.007\times10^{-5}(\pm3.946\times10^{-6})$***	$2.642\times10^{-5}(\pm4.107\times10^{-6})$***	$4.145\times10^{-4}(\pm2.818\times10^{-5})$
Scale × Slope	$-0.021(\pm3.215\times10^{-3})$***	-0.013 $(\pm3.822\times10^{-4})$***	$-0.012(\pm6.115\times10^{-4})$***	$-7.556\times10^{-3}(\pm3.643\times10^{-4})$***
Slope × Elevation × Aspect	$1.96\times10^{-4}(\pm7.578\times10^{-5})$**	$6.932\times10^{-6}(\pm1.387\times10^{-7})$	$-6.623\times10^{-5}(\pm2.134\times10^{-6})$**	$5.614\times10^{-5}(\pm2.606\times10^{-6})$***
Scale × Elevation × Slope	$3.652\times10^{-4}(\pm4.623\times10^{-5})$***	$8.246\times10^{-5}(\pm1.929\times10^{-6})$***	$6.598\times10^{-5}(\pm1.932\times10^{-6})$***	$6.568\times10^{-5}(\pm2.503\times10^{-6})$***
Scale × Slope × Aspect	$-3.807\times10^{-3}(\pm1.967\times10^{-3})$	$-1.179\times10^{-3}(\pm2.743\times10^{-4})$***	$2.041\times10^{-3}(\pm5.057\times10^{-4})$	$3.543\times10^{-3}(\pm2.777\times10^{-4})$